Int. J. Electrochem. Sci., 17 **(2022)** Article Number: 221136, doi: 10.20964/2022.11.36

International Journal of
ELECTROCHEMICAL
SCIENCE
www.electrochemsci.org

Rapid Electrochemical Detection of Heavy Metal Ions Pb^{2+} and Cd^{2+} in Petroleum Wastewater

Hongyong Ye, Guangling Zuo[*], *Rulin Li*

School of Biological and Chemical Engineering, Nanyang Institute of Technology, Nanyang 473004 China.
[*]E-mail: guanglingzuo@gmx.com

Received: 3 August 2022 / *Accepted:* 8 September 2022 / *Published:* 10 October 2022

The main heavy metal contaminants in petroleum wastewater are cadmium and lead ions, which have the greatest impact on humans. How to quickly and effectively detect heavy metals in petroleum wastewater is of practical importance. Co_3O_4 is a transition metal oxide with great potential for development. It has a high conductivity, good cycling stability and is relatively inexpensive to produce. In this work, we synthesized Co_3O_4 by hydrothermal method and characterized the morphology and structure of Co_3O_4 by X-ray diffraction and scanning electron microscopy. The synthesized Co_3O_4 can detect lead ions with high sensitivity after modification of the glassy carbon electrode. In addition, in the presence of lead ions, the proposed sensor can be used to detect cadmium ions at the same time. After optimization of the parameters, the sensor shows excellent detection performance. The proposed sensor has also been successfully used for the detection of cadmium and lead ions in petroleum wastewater.

Keywords: Electrochemical sensor; Square wave stripping voltammetry; Petroleum wastewater; Rapid detection; Co_3O_4

1. INTRODUCTION

Heavy metal ions such as lead and cadmium have serious biological toxicity and non-degradability, and are continuously enriched in the environment through the food chain and eventually enter the human body [1,2]. Heavy metal ions bind to a variety of enzymes and proteins in the human organism, rendering them inactive and causing the failure of most organs. Studies have found that when heavy metal ions in the human body accumulate to a certain level they can cause a variety of diseases and even cancer [3–5]. As the "blood" of modern industry, petroleum plays an important role in industrial production, transportation and other aspects. However, petroleum pollution cannot be ignored, including heavy metal ion pollution in petroleum wastewater has a greater risk. Petroleum wastewater consists of three main areas: drilling wastewater, refinery wastewater, and petrochemical wastewater[6–8].

According to statistics, about 12 million tons of waste drilling fluids are generated from oilfield drilling in China every year.

Cd^{2+} and Pb^{2+} are the most common heavy metal ions in petroleum wastewater. In a study of the Surig gas field block, heavy metal ions such as Cu^{2+}, Pb^{2+}, Hg^{2+}, Cr^{2+}, and Cd^{2+} were detected in the waste drilling fluids [9]. Their concentrations ranged from 0-30 μg/L, with Pb^{2+} concentrations around 7 μg/L and Cd^{2+} concentrations around 1 μg/L. Excess Cd^{2+} heavy metal concentrations were also found in water-based drilling fluid systems in the Tarim area [10]. It has also been reported that petroleum refinery wastewater contains up to 24 μg/L of Pb^{2+} and 2.7 μg/L of Cd^{2+} on average. The toxicogenic concentrations of Pb^{2+} and Cd^{2+} are very low for human health. The toxicogenic concentration of Pb^{2+} is 10-15 μg/L for infants and around 30 μg/L for adults [11]. A Cd^{2+} concentration of 0.2 μg/L can be harmful to humans. Cd^{2+} enters the body through the digestive and respiratory tracts and is excreted naturally at a very slow rate [12]. It accumulates in the body and can have a latency period of 10 to 30 years. It can damage the liver, kidneys, reproductive system, etc. It can develop strong carcinogenicity, which can cause tumors in certain areas [13]. After Pb^{2+} enters the body, only a small amount is excreted with metabolism, and most of it accumulates in the body. It can cause chronic diseases in the nerve, blood, and digestive systems, and even directly harm the nerve cells [14].

The most common excessive heavy metal ions Pb^{2+} and Cd^{2+} in petroleum wastewater directly or indirectly induce various diseases, which are mostly chronic diseases [15,16]. Therefore, the rapid detection of heavy metal ions by petroleum wastewater is an urgent problem to be solved [17,18]. The main detection techniques for heavy metals are atomic absorption spectrometry, inductively coupled plasma mass spectrometry, ultraviolet-visible spectrophotometry and electrochemical detection methods [19,20]. Among them, the principle of electrochemical detection method to detect a variety of heavy metal ions is mainly based on the occurrence of redox reactions between heavy metal ions. The most widely used electrochemical test method is the heavy metal plasma detection analysis using square wave stripping voltammetry (SWASV) [21–24]. The detection principle for heavy metal ions is mainly divided into two steps: (1) enrichment process: metal ion solution is deposited on the electrode through reduction reaction within a certain enrichment process. (2) Dissolution process: The deposited heavy metal monomers are re-oxidized under specific conditions and transformed into ions back into the solution [25–28].

As technology continues to innovate, new sensing materials are being developed. These new sensing composites are drop-coated on the surface of the working electrodes, thus enhancing the electrical properties [29,30]. This is mainly attributed to the superior physicochemical properties of the new nanocomposites. The new nanomaterials can be easily modified on the surface of the working electrode by certain functional groups and self-assembly properties, thus serving as sensing materials for detecting heavy metal ions [31,32]. Metal oxides with novel structures exhibit excellent physicochemical properties due to their unique morphology, varied dimensions, large specific surface area and catalytic activity [33–35]. Metal oxides have high mechanical strength and prevent wear and tear of the material. At the same time, they have a large specific surface area, which increases the active sites for the adsorption of heavy metal ions [36,37]. In addition, metal oxides have good biocompatibility, chemical stability and high electron conductivity, which can quickly and effectively adsorb heavy metal ions. With the advantages of high electrical conductivity, strong electron transfer

ability and strong adsorption ability for heavy metal ions, transition metal oxides have been widely used in electrochemical fields such as supercapacitors, anode materials for lithium-ion batteries and electrochemical sensors [38–40]. Cobalt has various valence states, among which Co_3O_4 is a transition metal oxide with great potential for development. It has a high conductivity, good cycling stability and is relatively inexpensive to produce. In this work, we synthesized cobalt-containing metal oxides for electrochemical detection of Cd^{2+} and Pb^{2+}.

2. EXPERIMENTAL

2.1. Chemicals

Cobalt nitrate was purchased from Tianjin Hedong District Hongyan Reagent Factory. Urea and ammonium fluoride were purchased from Tianjin Beichen Founder's Reagent Plant. Potassium chloride, anhydrous sodium acetate, glacial acetic acid were purchased from Kaifeng Fangjing Chemical Reagent Co. Potassium ferricyanide, potassium ferrocyanide was purchased from Tianjin Regent Chemicals Co. Disodium hydrogen phosphate, sodium dihydrogen phosphate was purchased from Luoyang Haohua Chemical Reagent Co. Lead nitrate and cadmium chloride were purchased from Tianjin Guangfu Fine Chemical Research Institute. Acetate buffer solutions (ABS) were used to detect heavy metal ions in the liquid phase.

2.2. Preparation of Co_3O_4 modified glassy carbon electrode (GCE)

Co_3O_4 particles were synthesized by hydrothermal method. Add 2 mM of cobalt nitrate, 15 mM of urea and 8 mM of ammonium fluoride to 40 mL of water. After 30 min of magnetic stirring and 10 min of sonication, the drug was completely dissolved to form a pink solution. The mixture was then transferred to a 50 mL PTFE reaction tank and reacted hydrothermally at 130 °C for 12 h. After the reaction was completed and cooled naturally to room temperature, the reactants were washed several times at room temperature and dried at 80°C for 10 h in a vacuum drying oven. Finally, the product was obtained by calcination in a tube furnace at 400°C for 3 h.

Disperse 5 mg of Co_3O_4 in 5 mL of water and sonicate for 10 min to form a homogeneous suspension. A certain amount of suspension drops are applied to the surface of the treated electrode with a pipette for modification, and the modified electrode is placed in air to dry.

2.3. Electrochemical measurement

A three-electrode system (GCE as working electrode, platinum sheet as auxiliary electrode, and saturated glycury electrode as reference electrode) was used for electrochemical detection. The electrochemical properties of the modified electrodes were characterized by cyclic voltammetry (CV) and electrochemical impedance spectroscopy (EIS) in 0.5 mM $K_3[Fe(CN)_6]$ solution containing 0.10 M KCl. In order to achieve optimal detection of heavy metals at the working electrode, the experimental

conditions should be optimized before the experiment. The current-time curve (i-t curve) was chosen for the accumulation process, and the accumulation voltage and accumulation current were determined under magnetic stirring conditions according to the optimization experiments. Optimization experiments were followed by the detection of certain concentrations of Pb^{2+} and Cd^{2+} by SWASV. The amplitude of SWASV was 25 mV; the step potential was 5 mV; and the frequency was 25 Hz. The electrode regeneration is the desorption of heavy metal ions from the electrodes. After the SWASV scan, the i-t curve was selected to clean the electrode surface. The cleaning process was held for 270 s at a potential setting of 0.2 V under magnetic stirring conditions.

3. RESULTS AND DISCUSSION

Figure 1 shows the SEM images before and after calcination of Co_3O_4. The material before calcination was $Co(OH)_2$, which mainly showed a round shape. The size of Co_3O_4 is in the range of 50-300 nm. The hydrothermal reaction at high temperature and pressure allows the solution in the reactor to react at a higher temperature than its boiling point, making it easy to control the particle size effectively and to obtain crystal particles of uniform size and shape [41,42]. The surface of Co_3O_4 showed a rough texture. After calcination, a part of the Co_3O_4 spheres showed a breakage and the hollow core could be seen. Meanwhile, the surface of Co_3O_4 further becomes rough, which increases the specific surface area of Co_3O_4 and provides more active sites for the adsorption of heavy metal ions in electrochemical detection [43].

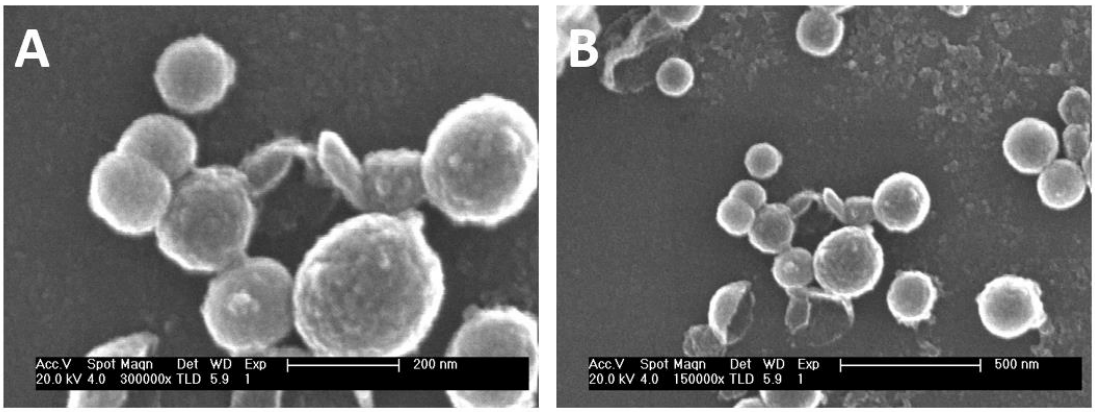

Figure 1. SEM images of (A) hydrothermal prepared $Co(OH)_2$ and (B) activated Co_3O_4.

We then analyzed the structure of the synthesized Co_3O_4 materials in depth by XRD. Figure 2 shows the XRD diffraction spectra of Co_3O_4. It can be seen that the characteristic peaks of the special material appear at 2θ angles of 19.01°, 31.26°, 36.84°, 38.53°, 44.80°, 55.65°, 59.35° and 65.23°, respectively, which are consistent with the standard diffraction pattern of Co_3O_4 at (111), (220), (311), (222), (400), (422), (511), and (440) in the standard diffraction pattern of Co_3O_4 (JCPDS No. 42-1467).

Moreover, the peak shapes of the characteristic peaks are sharp, indicating that the Co_3O_4synthesized by hydrothermal method with a high crystallinity [44]. In hydrothermal reactions, hydrolysis of urea can occur when the reaction temperature exceeds 90°C. The hydrolysis of urea is divided into two steps: first $CO(NH_2)_2$ is structurally alienated to ammonia cyanide (NH_4CNO) at high temperature. Then NH_4CNO is rapidly hydrolyzed to produce ammonium carbonate ($(NH_4)_2CO_3$). The hydrolysis of $(NH_4)_2CO_3$ produces OH-, resulting in a solution with a pH equal to approximately 9. In such an environment, it is favorable to generate a large amount of metal hydroxide precipitation and the resulting material is well crystallized [45]. During the synthesis of Co_3O_4, the generated OH- reacts with Co^{2+} to form $Co(OH)_2$ precipitate. The generated $Co(OH)_2$ is fully reacted with oxygen in the air at 400°C and oxidized to Co_3O_4.

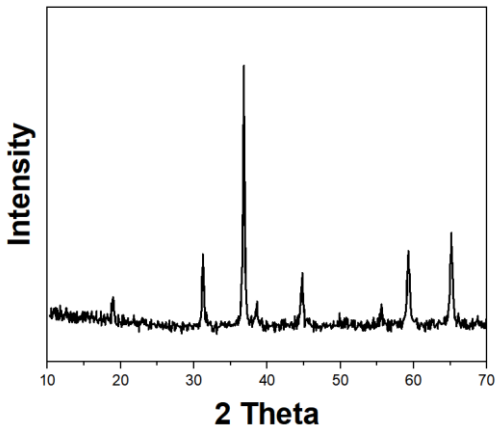

Figure 2. XRD pattern of synthesized Co_3O_4.

CV and EIS have a very important role in characterizing the modification of the working electrode surface. These two characterization can confirm whether the material is modified on the electrode or not, and can also obtain information on the degree of reversibility of the reaction on the electrode surface after modification of the functional material [46,47]. In this study, Co_3O_4/GCE was characterized electrochemically by CV and EIS in a solution of $K_3[Fe(CN)_6]$ containing KCl. Figure 3A and 3B show the CV and EIS results for GCE and Co_3O_4/GCE. As can be seen in Figure 3A, the values of the peak currents of the GCE oxidation and reduction peaks are around 65 μA, and the potential difference of the peak currents is around 65 mV. This indicates that the GCE itself has excellent electrical conductivity and electron transfer capability and is suitable for a conductive substrate [48]. The values of the peak currents of the Co_3O_4/GCE oxidation and reduction peaks decrease to about 45 μA, which is a decrease compared to the bare GCE, while the potential difference between the oxidation and reduction peaks increases to about 145 mV. This indicates that the electrode surface was successfully modified with Co_3O_4.

Figure 3B shows the Nyquist plots of GCE and Co_3O_4/GCE. The EIS curve consists of a half-circle part and a straight line part. The half-circle indicates the activation resistance of the material in the high frequency region. It represents the electron transfer process on the electrode surface and indicates

the electron transfer resistance (Rct) of that electrode surface. A larger diameter of the semicircle represents an increase in the resistance value [49]. The straight part represents the diffusion process at the electrode interface. A decreasing slope of the straight line represents a higher resistance value. As can be seen in Figure 3B, the GCE exhibits a semicircular arc with a very small diameter in the high frequency region of the Nyquist plot, indicating that the electron transport resistance on the GCE surface is very small and the electron transport rate is high [50]. The diameter of the semicircle in the high frequency region of the Co_3O_4/GCE is larger than that of the GCE in the high frequency region, indicating that the Co_3O_4 particles form a barrier on the surface of the GCE. The straight line in the low frequency region shows that these two lines are almost parallel before and after the electrode modification, indicating that the modification of Co_3O_4 has no effect on the diffusion process on the electrode surface. This is due to the fact that the high specific surface area of Co_3O_4 particles increases the contact area between the electrode/electrolyte phases and provides a large number of active sites for the reactions occurring on the electrode surface [51]. The electrochemical impedance curve of Co_3O_4/GCE shows that Co_3O_4 itself has good electrical conductivity.

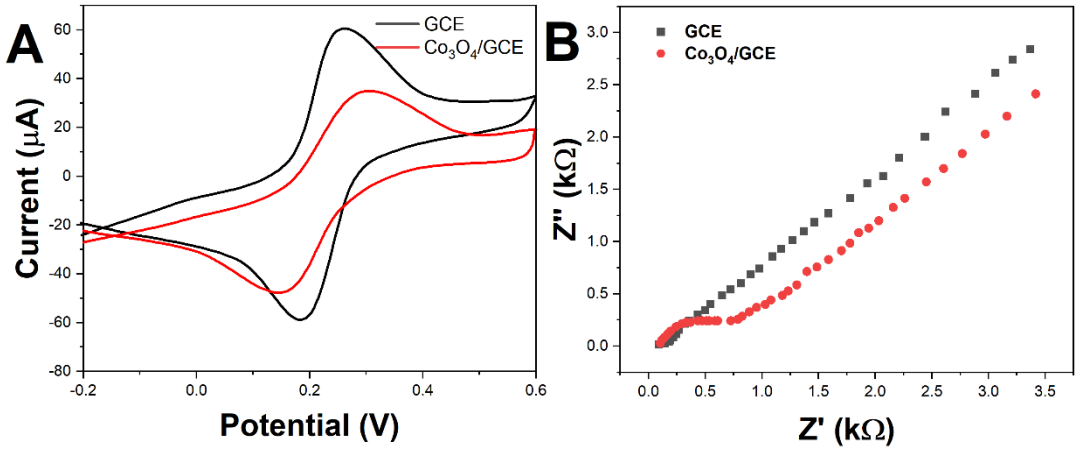

Figure 3. (A) CV and (B) EIS of GCE and Co_3O_4/GCE in 5 mM $K_3[Fe(CN)_6]$ with 0.5 M KCl. (CV scan rate: 50 mV/s)

GCE and Co_3O_4/GCE were tested towards 7 μM Cd^{2+} solution by SWASV at a deposition time of 240 s and a deposition voltage of -1.1 V in the ABS at pH 5.0. By comparing the intensity of the electrical signals collected by both, the reaction modified electrode has a certain sensitizing effect on the Cd^{2+} detection signal, and the experimental results are shown in Figure 4. As can be seen in Figure 4, the blank experiments showed no signal, which means that the electrical signals collected by both sensors are indeed Cd^{2+} detection signals. The GCE has a response signal to Cd^{2+} with a peak current Ip of 28.02 μA. The peak current of Co_3O_4/GCE is 65.47 μA. At the same time, the peak potential of Co_3O_4/GCE is -0.788 V, which is negatively shifted from -0.780 V of GCE. This indicates that Co_3O_4 has a significant sensitizing effect on Cd^{2+} detection. After Cd^{2+} adsorption on the Co_3O_4 surface, the binding energy of Cd_{3d} can be reduced by 0.8 eV compared to $Cd(NO_3)_2$. The decrease in binding energy was attributable

to the Cd^{2+} electron donated by the alkynyl group[52–54]. When Cd^{2+} ions containing empty orbitals were close to the surface of Co_3O_4, they would chelate with the electron-rich cobalt from Co_3O_4[52].

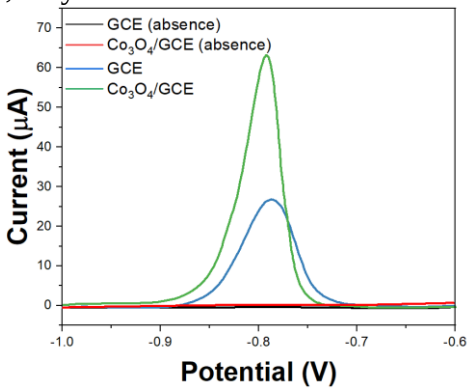

Figure 4. SWASV of GCE and Co_3O_4/GCE in the absence and presence of 7 μM Cd^{2+} (amplitude: 25 mV; step potential: 5 mV; frequency: 25 Hz).

We further optimized the buffer solutions. We chose ABS, phosphate buffer PBS and BR buffer for the test. At stronger alkalinity, the hydroxide ions in the solution form insoluble matter with cadmium ions [55,56], which affects the detection results. The three buffers tested were tested for the detection of Cd^{2+} in the acidic buffer range to determine the optimal buffer system and pH value. Figure 5A shows the detected electrical signals at pH 4.5, 5.0, 5.5, 6.0 and 6.5 of the BR buffer solution. In the BR buffer system, the detection signal increases and then decreases for different pH detection conditions. The maximum detection signal was reached at pH 5.0. Therefore, pH 5.0 was selected as the best test condition in the BR buffer.

The detection of Cd^{2+} was also performed in PBS buffer system. The pH 6.0, 6.5, 7.0, 7.5, and 8.0 were selected for the experiments, and the method and assay conditions were the same as above, and the results are shown in Figure 5B. From the figure, it can be seen that the detection signal increases and then decreases under different pH detection conditions in the PBS buffer system. The detection signal was maximized at pH 6.5. Therefore, pH 6.5 was selected as the best parameter in the PBS buffer system.

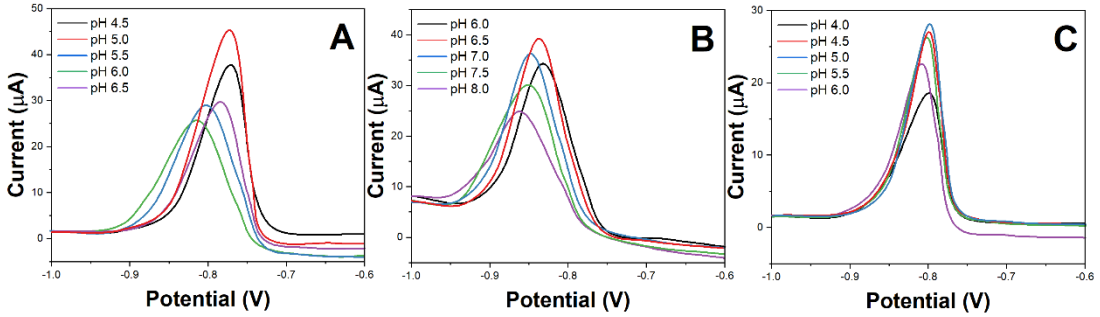

Figure 5. SWASV of Co_3O_4/GCE in (A) B-R buffer solution, (B) PBS and (C) ABS with different pH toward 5 μM Cd^{2+} (amplitude: 25 mV; step potential: 5 mV; frequency: 25 Hz).

The detection of Cd^{2+} was also carried out under ABS buffer system. The pH 3.75, 4.0, 4.5, 5.0, 5.5, and 5.75 were selected for the experiments, and the results are shown in Figure 5C. The peak current tends to increase and then decrease with increasing pH. The maximum value is reached when pH is 5.0. When pH>5.0, the increase of OH^- is not conducive to the stabilization of Cd^{2+}. When pH < 5.0, the solution is more acidic, which is not conducive to the stabilization of the electrode surface film. Therefore, pH 5.0 was selected as the optimal condition for Cd^{2+} detection in the experiment when ABS buffer was used as the supporting buffer. Comparing the three buffer solutions, Co_3O_4/GCE in the ABS buffer system at pH 5.0 showed a best detection signal for Cd^{2+}.

We further optimized the accumulation potential. The accumulation potential were -0.9 V, -1.0 V, -1.1 V, -1.2 V, -1.3 V, and -1.4 V. The experimental results are shown in Figure 6. As the accumulation potential increases, the peak current tends to increase first and then decrease. The peak current reaches a maximum at an accumulation potential of -1.1V. When the accumulation potential is less than -1.1 V, the more Cd^{2+} is reduced on the electrode surface as the accumulation potential increases, resulting in the enhancement of the electrical signal and the increase of the peak current during the dissolution phase [57]. When the accumulation potential is greater than -1.1 V, bubbles appear on the electrode surface during the experimental process, probably due to the generation of gas by electrolysis. The accumulation of bubbles on the surface of the electrode interferes more with the redox of Cd^{2+} and thus reduces the peak current. Therefore, -1.1 V was selected as the optimal accumulation potential for the detection of Cd^{2+} in the experiment.

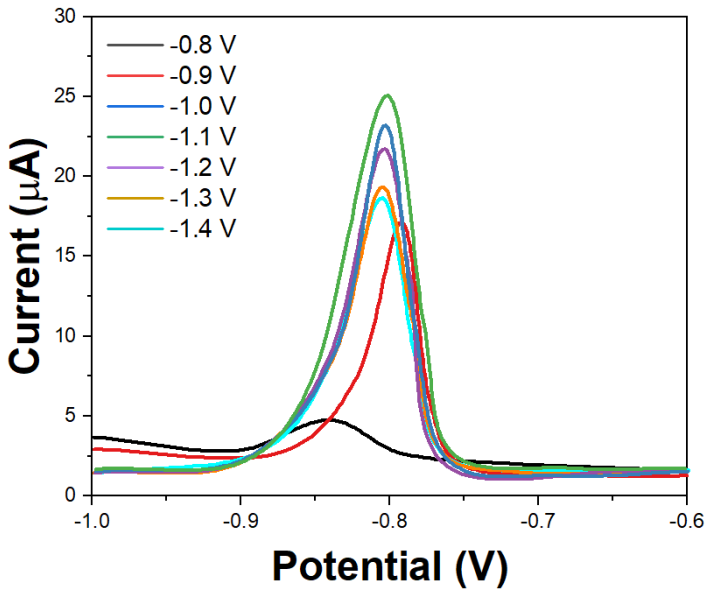

Figure 6. SWASV of Co_3O_4/GCE towards 3 μM Cd^{2+} detection with different accumulation potential (amplitude: 25 mV; step potential: 5 mV; frequency: 25 Hz).

The time of accumulation can also affect the detection. Figure 7 shows the detection results of Co_3O_4/GCE for 3 μM Cd^{2+} at 120s, 180s, 240s, 300s, 360s, 420s, 480s, and 540s accumulation. There

is a tendency for the peak current to increase all the time with increasing accumulation time. The increase in current decreases after 240 s and then plateaus. During the accumulation process, as the time increases, more Cd^{2+} ions are reduced on the surface of the electrode thus increasing the electrical signal during the solubilization phase [58]. Therefore, we choose 240s as the optimal accumulation time.

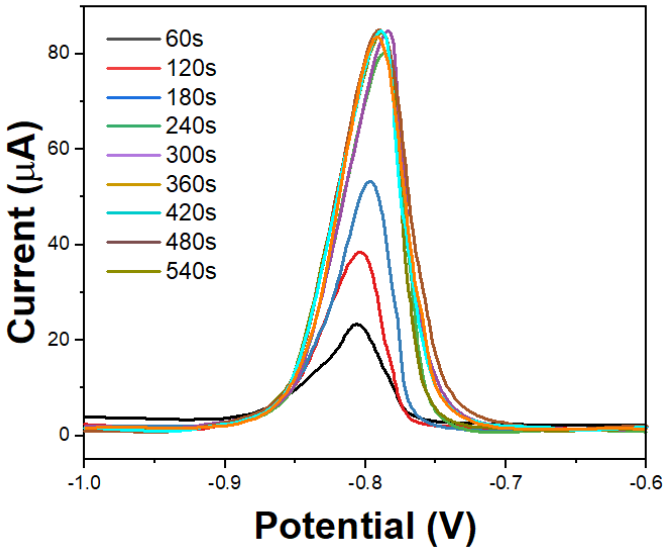

Figure 7. SWASV of Co_3O_4/GCE towards 3 μM Cd^{2+} detection with different accumulation time (amplitude: 25 mV; step potential: 5 mV; frequency: 25 Hz).

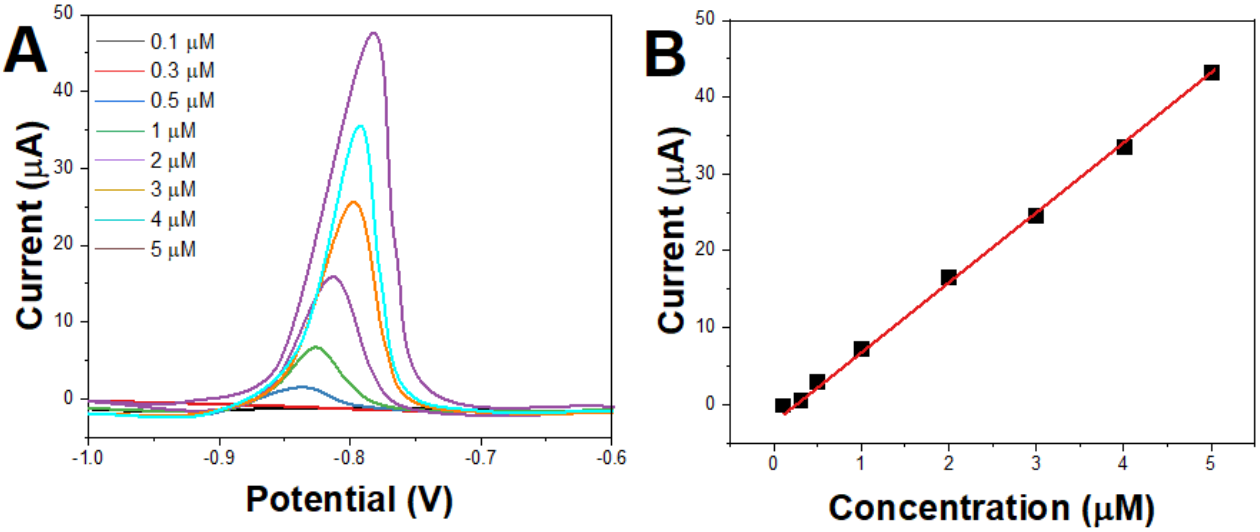

Figure 8. (A) SWASV and (B) relationship plots of Co_3O_4/GCE towards different concentrations of Cd^{2+} (amplitude: 25 mV; step potential: 5 mV; frequency: 25 Hz).

Under optimal conditions, we determined the range of linearity of the Cd^{2+} ion detection signal. Figure 8 shows the detection curves of Co_3O_4/GCE for 0.1-5 μM Cd^{2+}. In this range Co_3O_4/GCE showed a good linear relationship between the detection current and the Cd^{2+} concentration. The detection limit can be calculated as 50 nM.

We further explored the detection performance of Pb^{2+} by the presence of Cd^{2+}. We fixed the Cd^{2+} concentration at 1 μM and varied the Pb^{2+} concentration. Figure 9 shows the SWASV of Co_3O_4/GCE for the detection of two heavy metal ions, and the results show a good linearity between 10 nM and 4 μM for Pb^{2+}. The detection limit was calculated as 4 nM.

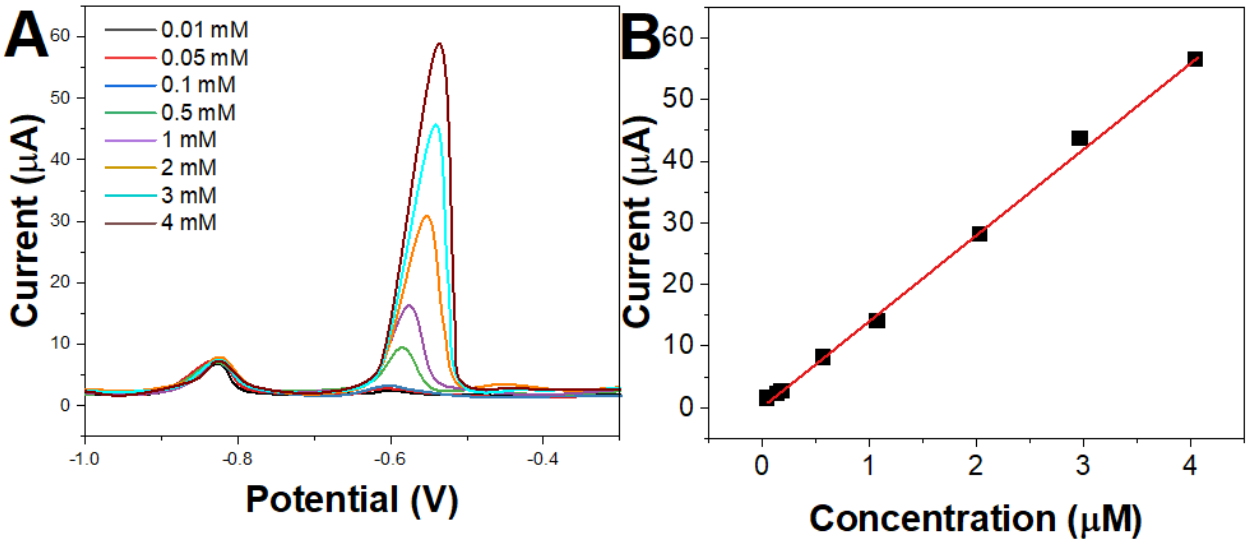

Figure 9. (A) SWASV and (B) relationship plots of Co_3O_4/GCE towards different concentrations of Pb^{2+} in the presence of 1 μM. of Cd^{2+} (amplitude: 25 mV; step potential: 5 mV; frequency: 25 Hz).

We also explored the detection performance of Cd^{2+} by the presence of Pb^{2+}. We fixed the Pb^{2+} concentration at 1 μM and varied the Cd^{2+} concentration. Figure 10 shows the SWASV of Co_3O_4/GCE for the detection of two heavy metal ions, and the results show a good linearity between 0.1 and 4 μM for Cd^{2+}. The detection limit was calculated as 45 nM.

The established method of detection was applied to the simulated petroleum effluent treatment and the results are shown in Table 1. We validated the results of the assay with spiked recoveries. The experimental results demonstrate the potential of the proposed electrochemical sensor to be applied for the detection of lead and cadmium ions in petroleum wastewater.

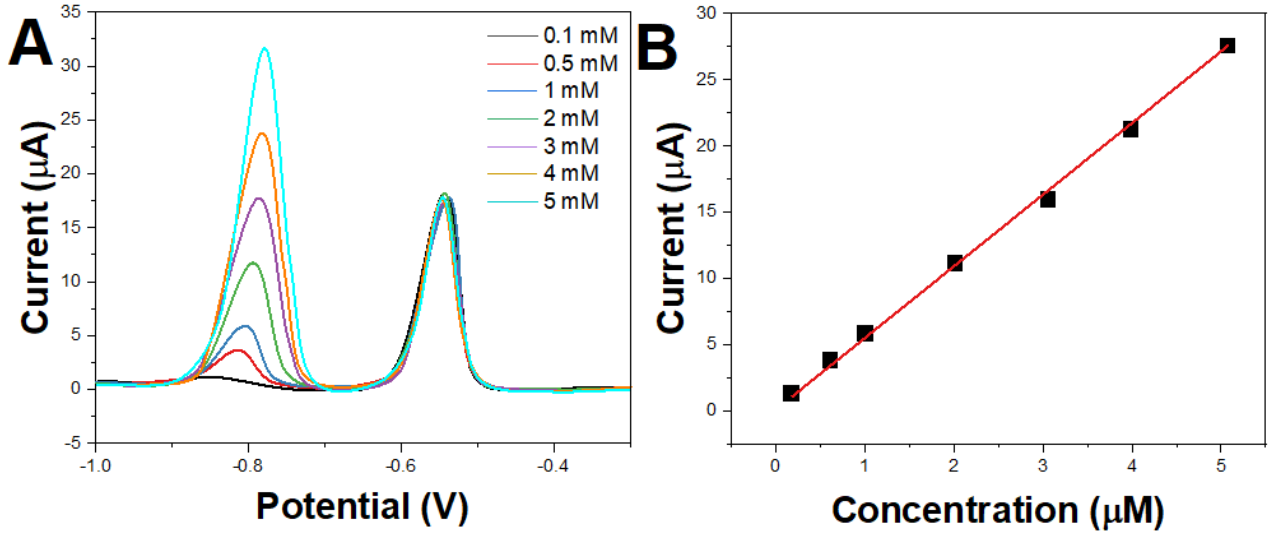

Figure 10. (A) SWASV and (B) relationship plots of Co_3O_4/GCE towards different concentrations of Cd^{2+} in the presence of 1 μM of Pb^{2+} (amplitude: 25 mV; step potential: 5 mV; frequency: 25 Hz).

Table 1. Real sample test using proposed Co_3O_4/GCE towards petroleum wastewater using SWASV.

Sample	Cd^{2+} detection	Pb^{2+} detection	Cd^{2+} Addition	Pb^{2+} Addition	Cd^{2+} detection	Pb^{2+} detection	Cd^{2+} Recovery (%)	Pb^{2+} Recovery (%)
1	1.44 μM	0.67 μM	0.50 μM	0.50 μM	1.90 μM	1.93 μM	97.94	99.48
2	1.31 μM	0.66 μM	1.00 μM	1.00 μM	2.25 μM	2.41 μM	97.40	104.33
3	1.42 μM	0.63 μM	1.50 μM	1.50 μM	3.04 μM	2.94 μM	104.44	100.68

4. CONCLUSION

In this work, we synthesized Co_3O_4 particles by hydrothermal method for the modification of GCE. The prepared Co_3O_4/GCE has good electrical conductivity and the microstructure of the electrode surface provides more active sites for electroanalytical probes. The modified electrometer combined with SWASV can be used to detect lead and cadmium ions in petroleum wastewater. After optimizing the electrolyte, deposition time and deposition potential, Co_3O_4/GCE can achieve highly sensitive detection of Pb and Cd ions. The proposed electrochemical sensor was also successfully used for the detection of lead and cadmium ions in petroleum wastewater.

References

1. X. Wang, Y. Qi, Y. Shen, Y. Yuan, L. Zhang, C. Zhang, Y. Sun, *Sensors and Actuators B: Chemical*, 310 (2020) 127756.
2. B. Unnikrishnan, C.-W. Lien, H.-W. Chu, C.-C. Huang, *Journal of Hazardous Materials*, 401 (2021) 123397.
3. Z. Xu, Z. Liu, M. Xiao, L. Jiang, C. Yi, *Chemical Engineering Journal*, 394 (2020) 124966.
4. N.S.M. Ramdzan, Y.W. Fen, N.A.A. Anas, N.A.S. Omar, S. Saleviter, *Molecules*, 25 (2020) 2548.
5. Q. Ding, C. Li, H. Wang, C. Xu, H. Kuang, *Chemical Communications*, 57 (2021) 7215–7231.
6. C. Wu, M. Wang, Z. Yu, H. Gao, *Journal of Water Process Engineering*, 49 (2022) 103019.
7. B.N. Thorat, R.K. Sonwani, *Bioresource Technology* (2022) 127263.
8. K. Ghezali, N.B. Tahar, G. Otmanine, N. Guettaf, *Journal of Environmental Treatment Techniques*, 10 (2022) 18–23.
9. S.A. Younis, H.A. Maitlo, J. Lee, K.-H. Kim, *Advances in Colloid and Interface Science*, 275 (2020) 102071.
10. A. Ahmad, *Environmental Science and Pollution Research*, 29 (2022) 5777–5786.
11. E. Ituen, L. Yuanhua, C. Verma, A. Alfantazi, O. Akaranta, E.E. Ebenso, *Journal of Molecular Liquids*, 335 (2021) 116132.
12. S. Varjani, R. Joshi, V.K. Srivastava, H.H. Ngo, W. Guo, *Environmental Science and Pollution Research*, 27 (2020) 27172–27180.
13. S.T. Malkapuram, V. Sharma, S.P. Gumfekar, S. Sonawane, S. Sonawane, G. Boczkaj, M.M. Seepana, *Sustainable Energy Technologies and Assessments*, 48 (2021) 101576.
14. M.S. Kuyukina, A.V. Krivoruchko, I.B. Ivshina, *Applied Sciences*, 10 (2020) 831.
15. X. He, K. Jia, Y. Bai, Z. Chen, Y. Liu, Y. Huang, X. Liu, *Journal of Hazardous Materials*, 405 (2021) 124263.
16. A. Numan, A.A. Gill, S. Rafique, M. Guduri, Y. Zhan, B. Maddiboyina, L. Li, S. Singh, N.N. Dang, *Journal of Hazardous Materials*, 409 (2021) 124493.
17. T.V. Wagner, F. Al-Manji, J. Xue, K. Wetser, V. de Wilde, J.R. Parsons, H.H. Rijnaarts, A.A. Langenhoff, *Environmental Science and Pollution Research*, 28 (2021) 2172–2181.
18. I. Haq, A.S. Kalamdhad, *Environmental Technology & Innovation*, 23 (2021) 101651.
19. R. Sivakumar, N.Y. Lee, *Chemosphere*, 275 (2021) 130096.
20. A. Nain, Y.-T. Tseng, Y.-S. Lin, S.-C. Wei, R.P. Mandal, B. Unnikrishnan, C.-C. Huang, F.-G. Tseng, H.-T. Chang, *Sensors and Actuators B: Chemical*, 321 (2020) 128539.
21. J.-J. Ye, C.-H. Lin, X.-J. Huang, *Journal of Electroanalytical Chemistry*, 872 (2020) 113934.
22. M.-S. Koshki, M. Baghayeri, M. Fayazi, *Journal of Food Measurement and Characterization*, 15 (2021) 5318–5325.
23. S.E.D. Bahinting, A.P. Rollon, S. Garcia-Segura, V.C.C. Garcia, B.M.B. Ensano, R.R.M. Abarca, J.-J. Yee, M.D.G. de Luna, *Sensors*, 21 (2021) 1811.
24. P. Sanchayanukun, S. Muncharoen, *Talanta*, 217 (2020) 121027.
25. N. Liu, G. Zhao, G. Liu, *Sensors*, 20 (2020) 6792.
26. S.E. Berrabah, A. Benchettara, F. Smaili, S. Tabti, A. Benchettara, *Materials Chemistry and Physics*, 278 (2022) 125670.
27. S. Phal, H. Nguyễn, A. Berisha, S. Tesfalidet, *Sensing and Bio-Sensing Research*, 34 (2021) 100455.
28. J. Pizarro, R. Segura, D. Tapia, F. Navarro, F. Fuenzalida, M.J. Aguirre, *Food Chemistry*, 321 (2020) 126682.
29. J. Guan, Y. Fang, T. Zhang, L. Wang, H. Zhu, M. Du, M. Zhang, *Electrocatalysis*, 11 (2020) 59–67.
30. H.A. Hamid, Z. Lockman, N.M. Nor, N.D. Zakaria, K.A. Razak, *Materials Chemistry and Physics*, 273 (2021) 125148.
31. Y. Zhang, C. Li, Y. Su, W. Mu, X. Han, *Inorganic Chemistry Communications*, 111 (2020) 107672.
32. A. Scandurra, S. Mirabella, *IEEE Sensors Journal*, 21 (2021) 22134–22142.

33. H. Karimi-Maleh, M. Alizadeh, Y. Orooji, F. Karimi, M. Baghayeri, J. Rouhi, S. Tajik, H. Beitollahi, S. Agarwal, V.K. Gupta, S. Rajendran, S. Rostamnia, L. Fu, F. Saberi-Movahed, S. Malekmohammadi, *Ind. Eng. Chem. Res.*, 60 (2021) 816–823.
34. H. Karimi-Maleh, A. Ayati, R. Davoodi, B. Tanhaei, F. Karimi, S. Malekmohammadi, Y. Orooji, L. Fu, M. Sillanpää, *Journal of Cleaner Production*, 291 (2021) 125880.
35. H. Karimi-Maleh, A. Ayati, S. Ghanbari, Y. Orooji, B. Tanhaei, F. Karimi, M. Alizadeh, J. Rouhi, L. Fu, M. Sillanpää, *Journal of Molecular Liquids*, 329 (2021) 115062.
36. T. Zhang, Q. Liu, X. Wei, Z. Jiang, T. Cui, *Sensors and Actuators B: Chemical*, 311 (2020) 127948.
37. Q. Yang, B. Nagar, R. Alvarez-Diduk, M. Balsells, A. Farinelli, D. Bloisi, L. Proia, C. Espinosa, M. Ordeix, T. Knutz, *ACS Es&t Water*, 1 (2021) 2470–2476.
38. H. Karimi-Maleh, H. Beitollahi, P.S. Kumar, S. Tajik, P.M. Jahani, F. Karimi, C. Karaman, Y. Vasseghian, M. Baghayeri, J. Rouhi, *Food and Chemical Toxicology* (2022) 112961.
39. H. Karimi-Maleh, C. Karaman, O. Karaman, F. Karimi, Y. Vasseghian, L. Fu, M. Baghayeri, J. Rouhi, P. Senthil Kumar, P.-L. Show, S. Rajendran, A.L. Sanati, A. Mirabi, *Journal of Nanostructure in Chemistry*, 12 (2022) 429–439.
40. H. Karimi-Maleh, F. Karimi, L. Fu, A.L. Sanati, M. Alizadeh, C. Karaman, Y. Orooji, *Journal of Hazardous Materials*, 423 (2022) 127058.
41. M. Majidian, J.B. Raoof, S.R. Hosseini, R. Ojani, J. Barek, J. Fischer, *Electroanalysis*, 32 (2020) 2260–2265.
42. S. Slimi, H. Barhoumi, N. Jaffrezic-Renault, *Sensor Letters*, 18 (2020) 811–818.
43. M. Nodehi, M. Baghayeri, H. Veisi, *Talanta*, 230 (2021) 122288.
44. Y. He, Z. Wang, L. Ma, L. Zhou, Y. Jiang, J. Gao, *RSC Advances*, 10 (2020) 27697–27705.
45. J.G. Walters, S. Ahmed, I.M. Terrero Rodríguez, G.D. O'Neil, *Electroanalysis*, 32 (2020) 859–866.
46. D.J. Arnot, T.N. Lambert, *Electroanalysis*, 33 (2021) 797–803.
47. X.-Y. Lin, Q.-W. Zhou, X.-L. Huo, N. Bao, *Microchemical Journal*, 179 (2022) 107428.
48. J. Lee, S. Kim, H. Shin, *Sensors*, 21 (2021) 1346.
49. L. Durai, S. Badhulika, *Sensors and Actuators Reports*, 4 (2022) 100097.
50. M. Nodehi, M. Baghayeri, A. Kaffash, *Chemosphere*, 301 (2022) 134701.
51. J. Lee, S. Kim, H. Shin, *Sensors*, 21 (2021) 1346.
52. R. Liu, J. Zhou, X. Gao, J. Li, Z. Xie, Z. Li, S. Zhang, L. Tong, J. Zhang, Z. Liu, *Advanced Electronic Materials*, 3 (2017) 1700122.
53. X.-Y. Xiao, S.-H. Chen, S.-S. Li, J. Wang, W.-Y. Zhou, X.-J. Huang, *Environ. Sci.: Nano*, 6 (2019) 1895–1908.
54. Y.-F. Sun, P.-H. Li, M. Yang, X.-J. Huang, *Sensors and Actuators B: Chemical*, 292 (2019) 136–147.
55. N.I. Hrastnik, V. Jovanovski, S.B. Hočevar, *Sensors and Actuators B: Chemical*, 307 (2020) 127637.
56. L. Oularbi, M. Turmine, F.E. Salih, M. El Rhazi, *Journal of Environmental Chemical Engineering*, 8 (2020) 103774.
57. S. Sawan, R. Maalouf, A. Errachid, N. Jaffrezic-Renault, *TrAC Trends in Analytical Chemistry*, 131 (2020) 116014.
58. C. Yıldız, D.E. Bayraktepe, Z. Yazan, M. Önal, *Journal of Electroanalytical Chemistry*, 910 (2022) 116205.